MICROPLANE MODEL FOR BRITTLE-PLASTIC MATERIAL: II. VERIFICATION

By Zdeněk P. Bažant,[1] Fellow, ASCE, and Pere C. Prat,[2] Student Member, ASCE

ABSTRACT: The general microplane model formulated in Part I of this study is calibrated and verified by comparison with numerous nonlinear triaxial test data from the literature and good agreement is achieved. The model involves many fewer material parameters than the previous phenomenologic macroscopic models. Numerical implementation is also considered.

INTRODUCTION

In Part I, which immediately precedes this paper, a general microplane model for brittle-plastic materials such as concrete has been developed. The objective of Part II is to calibrate and verify this model by comparisons with the basic experimental data that exist in the literature and to discuss numerical implementation. All the definitions and notations from Part I of this study are retained.

The data from various basic material tests have been fitted directly by solving Eq. 13 of Part I, which represents a system of six algebraic equations relating the stress and strain increments. These equations have been rearranged so that the controlled strain or stress components appear on the right-hand side, and the measured ones appear on the left-hand side. Various standard rules required for stability of computations (Bažant and Shieh 1978) have been observed (e.g., in the strain-softening range one must prescribe the increments of the major axial strain rather than the axial stress; in proportional triaxial tests one must implement a prescribed ratio of the strain increments in various directions, etc.).

EMPIRICAL MATERIAL FUNCTIONS

For the functions defining the microplane secant moduli C_V, C_D, and C_T, the following expressions have been obtained intuitively and verified experimentally:

$$\text{for } \varepsilon_V \geq 0: \quad C_V = C_V^0 e^{-|\varepsilon_V/a_1|^{p_1}} \tag{1}$$

$$\text{for } \varepsilon_V < 0: \quad C_V = C_V^0 \left[\left(1 + \left| \frac{\varepsilon_V}{a} \right| \right)^{-p} + \left| \frac{\varepsilon_V}{b} \right|^q \right] \tag{2}$$

[1]Prof. of Civ. Engrg., Dept. of Civ. Engrg., Northwestern Univ., Evanston, IL 60208.

[2]Res. Assoc., Materials Sci. Inst. (CSIC), Barcelona, Spain; formerly, Grad. Res. Asst., Northwestern Univ.

Note. Discussion open until March 1, 1989. Separate discussions should be submitted for the individual papers in this symposium. To extend the closing date one month, a written request must be filed with the ASCE Manager of Journals. The manuscript for this paper was submitted for review and possible publication on August 7, 1987. This paper is part of the *Journal of Engineering Mechanics*, Vol. 114, No. 10, October, 1988. ©ASCE, ISSN 0733-9399/88/0010-1689/$1.00 + $.15 per page. Paper No. 22824.

$$\text{for } \varepsilon_D \geq 0: \quad C_D = D_D^0 e^{-|\varepsilon_D/a_1|^{p_1}} \tag{3}$$

$$\text{for } \varepsilon_D < 0: \quad \begin{cases} C_D = C_D^0 e^{-|\varepsilon_D/a_2|^{p_2}} & (4) \\ C_T = C_T^0 e^{-|\varepsilon_T/a_5|^{p_3}} & (5) \end{cases}$$

in which

$$a_5 = a_3 \quad \text{if } \sigma_C \geq 0 \tag{6a}$$

$$a_5 = a_3 - \frac{a_4}{f_c'} \sigma_C \quad \text{if } \sigma < 0 \tag{6b}$$

in which a, b, p, q, a_1, a_2, a_3, a_4, p_1, p_2, and p_3 are positive empirical material constants. The dependence of a_5 on the confining stress σ_C reflects internal friction and represents an additional static constraint of nontensorial (scalar) type.

The expression for C_V in compression (Eq. 2) can be obtained independently of all others, by simple curve fitting of the test data for hydrostatic compression of the material. As is well known, the hydrostatic compression response exhibits neither maximum stress nor strain softening. Rather, it follows a curve of the shape sketched in Fig. 2(*b*) of Part I. Under hydrostatic loading ($\sigma_{11} = \sigma_{22} = \sigma_{33} = \sigma_V$, $\sigma_{12} = \sigma_{23} = \sigma_{31} = 0$), the stress-strain relation for the microplane system reduces to the simple equation $\sigma_V = C_V \varepsilon_V$ where σ_V now represents the volumetric (or hydrostatic, or mean) stress, $\sigma_V = \sigma_{kk}/3$.

Parameters a, b, p, and q may be identified independently of the others. This can be done by the fitting of one curve to the hydrostatic test data. The fitting can be easily accomplished by a trial-and-error approach. Alternatively, a good fit can be achieved by a nonlinear optimization algorithm such as the Levenberg-Marquardt is, which yields the values of the parameters a, b, p, and q. As still another alternative, one can make trial-and-error choices of only parameters a and p, and then identify parameters b and q by linear regression, plotting log Y vs. log ε_V where $Y = (C_V/C_V^0) - (1 + |\varepsilon_V/a|)^{-p}$; this plot is ideally linear (i.e., $\log Y = q \log \varepsilon_V - q \log b$, with slope q and vertical intercept $q \log b$).

The expressions for C_V, C_D, and C_T in Eqs. 1 and 3–5 are perhaps the simplest expressions that yield, for each stress-strain diagram for the microplane, a curve of the shape shown in Fig. 2(*c*) of Part I. According to these formulas, the strain-softening tail approaches zero stress asymptotically, as the strains approach infinity. Such a shape of the strain-softening curve has been assumed by many investigators, although test data for strain softening at very large strains, with stress less than about 15% of the peak stress, do not seem to exist.

In this regard it may be noted that in recent micromechanics analysis of the crack ligament tearing (Bažant 1987) it appeared that strain softening should terminate at a certain maximum strain after which the stress-strain curve exhibits snapback behavior (i.e., returns to the origin with positive slope) [see the dashed curve in Fig. 2(*c*) of Part I]. A modification of Eqs. 1 and 3–5 in this sense might have to be introduced in the future, but in the present fitting of test data the foregoing simple expressions were used for the sake of simplicity since a curve with a maximum strain would cause

numerical complications. This is of little practical consequence for the present analysis because the existing test data do not go into large enough strains for which the snapback after maximum strain [the dashed curve in Fig. 2(*c*) of Part I] would be reached.

Analysis of numerous test data reveals that the optimum values of exponents p_1, p_2, and p_3 are always nearly the same and can be fixed as follows:

$$p_1 = 0.5 \quad \ldots\ldots (7a)$$

$$p_2 = p_3 = 1.5 \quad \ldots\ldots (7b)$$

Parameters a, b, p, and q are also nearly the same for all concretes and can anyway be identified separately from the single hydrostatic test curve. The elastic properties can also be determined in advance separately. This leaves only five material parameters, a_1, a_2, a_3, a_4 and η_0, to be identified by simultaneous fitting of the test data for uniaxial and multiaxial loadings.

The values of the two elastic constants, Poisson's ratio ν and Young's modulus E, are fixed prior to the data fitting. The Poisson ratio is assumed to be $\nu = 0.18$ for all the cases, and the Young's modulus is chosen such that the initial slope of the curves obtained with the model fit the experimental data.

Verification with Experimental Results

Fits of various typical test data from the literature (Balmer 1949; Bažant et al. 1986; Bresler and Pister 1958; Goode and Helmy 1967; Green and Swanson 1973; Hognestad et al. 1955; Kotsovos and Newman 1978; Kupfer et al. 1969; Launay and Gachon 1971; Lin et al. 1987; Petersson 1981; Sinha et al. 1964; van Mier 1984) are exhibited in Figs. 1–10. The measurements are shown as the data points while the results of the present model are plotted as the solid curves. The failure envelopes in Figs. 8 and 9 have been constructed by simulating various standard triaxial and biaxial tests, respectively, and recording the maximum stress value for each test. Collecting these maximum stress values then provides the failure envelope. The basic information on most of these tests is summarized in Bažant and Shieh (1978) and Lin et al. (1987).

The optimum values of the material parameters corresponding to each of these fits are listed in Tables 1 and 2. The optimization by which the fits have been achieved was carried out simply by a trial-and-error approach. If all the data fits were optimized collectively, the scatter of the parameter values from one test series to another would probably be much less than that in Tables 1 and 2. More sophisticated computer optimization would be needed for that purpose.

The fits achieved with the present model are closer than those achieved previously with various phenomenologic macroscopic models. At the same time, the number of the free material parameters to be identified from the test data is greatly reduced. While the previous models that could reasonably approximate the present data required (in addition to two elastic constants) at least 15 material parameters to be identified from the measured data, the present model involves only five such material parameters, aside from further four parameters which are identified in advance

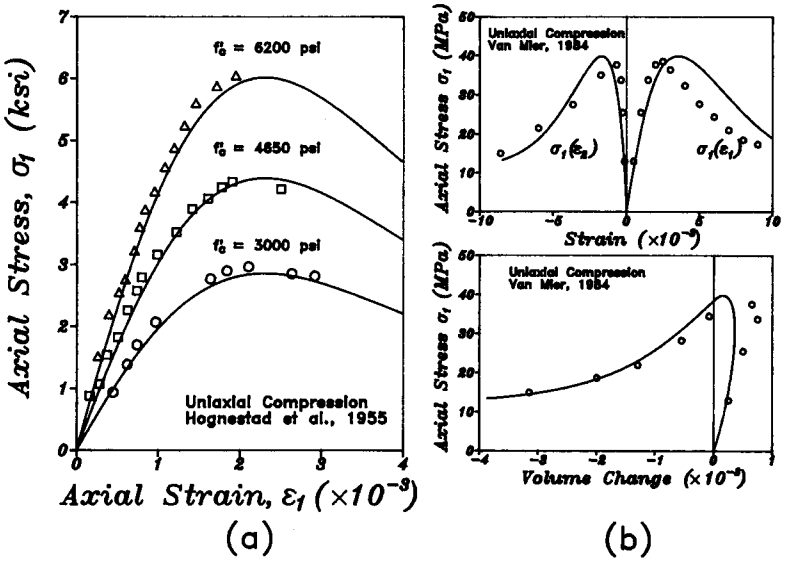

FIG. 1. Comparison with Uniaxial Compression Tests, Reported by: (*a*) Hognestad et al. (1955); (*b*) Van Mier (1984)

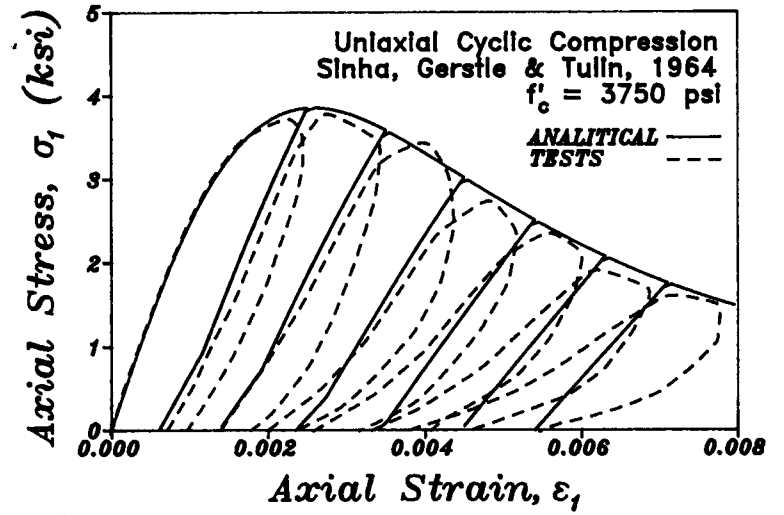

FIG. 2. Comparison with Uniaxial Cyclic Compression Tests, Reported by Sinha et al. (1964)

by simple curve fitting of the hydrostatic test and can be assumed in advance if the hydrostatic test reaching very high pressures is unavailable.

So we achieve a significant simplification of the numerical work needed to identify the material parameters. At the same time we achieve signifi-

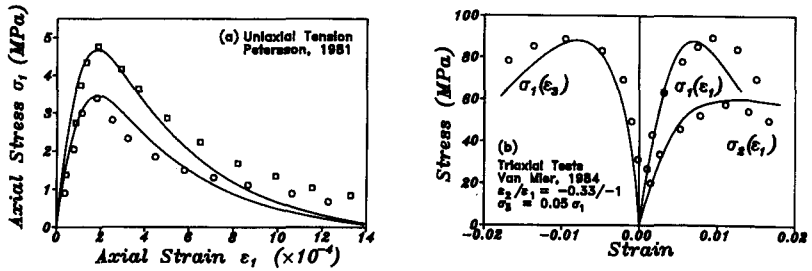

FIG. 3. Comparison with: (*a*) Uniaxial Tension Tests, Reported by Petersson (1981); (*b*) True Triaxial Tests, Reported by Van Mier (1984)

cant conceptual simplification. This is of course at the expense of extensive numerical work that has to be done by the computer when the present model is used in finite element analysis. However, with the recent advances in computing speed and power, this is no longer a serious obstacle [e.g., if the spherical integration formula with 21 microplanes is used, then one needs to store in the computer's memory 132 numbers for each integration point of each finite element (i.e., three stresses and three strain maxima per microplane, and six macrostrains); for the formula with 16 microplanes, this becomes 102 instead of 132].

From the fits shown in Figs. 1–10 it is obvious that the model can describe the major characteristics of the response of a brittle-plastic material such as concrete. This includes the progressive strain softening

TABLE 1. Optimum Values of Material Parameters: Basic Parameters

Test data (1)	η_0 (2)	a_1 ($\times 10^{-4}$) (3)	a_2 ($\times 10^{-3}$) (4)	a_3 (5)	a_4 (6)
Balmer	0.85	5.0	2.5	0.0018	0.0100
Bažant et al.	1.00	5.0	1.0	0.0010	0
Green et al.	1.00	4.0	2.0	0.0017	0
Hognestad et al.	0.50	5.0	2.5	0.0015	0
Kotsovos & Newman	0.85	5.0	5.0	0.0100	0.0160
Kupfer et al.	0.60	1.0	5.0	0.0011	0.0009
Petersson	0.25	0.3	0.5	0.0005	0
Sinha et al.	0.50	5.0	3.2	0.0016	0
van Mier	0.85	4.0	4.3	0.0018	0.0020

TABLE 2. Optimum Values of Material Parameters: Hydrostatic Curve Parameters

Test data (1)	a (2)	b (3)	p (4)	q (5)
Bažant et al.[a]	0.0050	0.0435	0.50	2.00
Bažant et al.[b]	0.0002	0.0850	0.36	3.00
Green & Swanson[c]	0.0008	0.1000	0.50	1.80
All Other Test Data	0.0050	0.2250	0.25	2.25

[a]Very high confining stress, small aggregate concrete.
[b]Very high confining stress, cement paste.
[c]High-strength concrete.

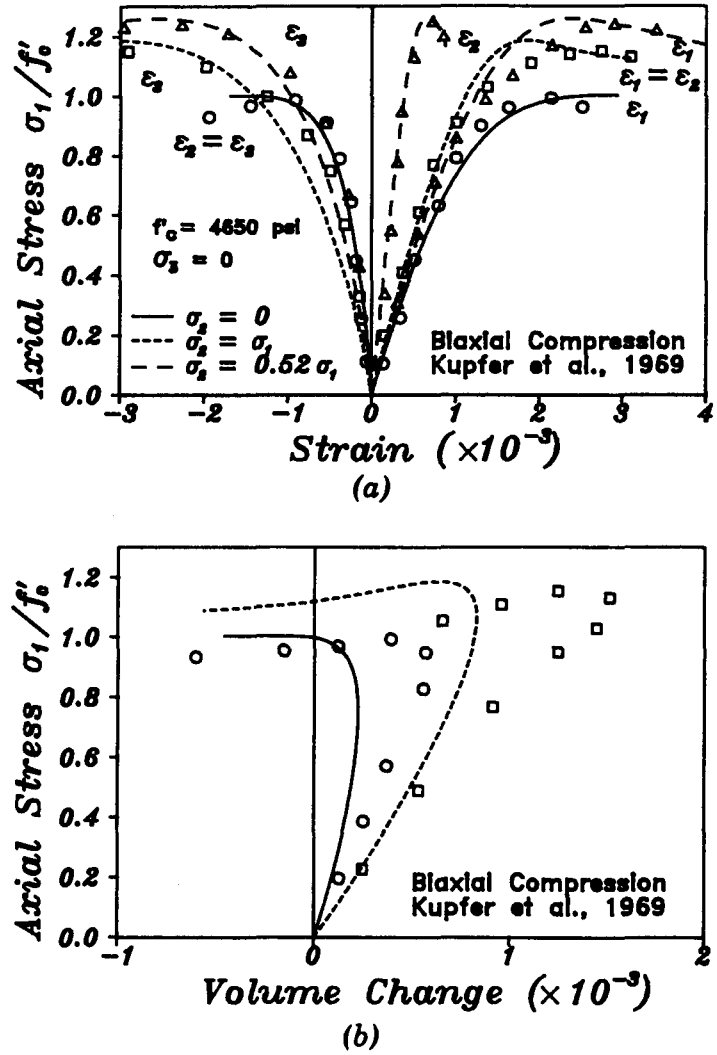

FIG. 4. Comparison with Biaxial Tests, Reported by Kupfer et al. (1969)

with a long tail, large-volume expansion due to strain softening in uniaxial as well as triaxial tests; transition from brittle response at small hydrostatic pressure to essentially plastic hardening response at high hydrostatic pressures; the absence of stress maximum in the hydrostatic pressure test; the difference in the shape of the compressive and tensile meridians in the Rendulić (volumetric) section of the failure envelope (Fig. 8); the rounded triangular shape in the deviatoric cross sections of the failure surface (Fig. 8); including a transition to a more circular shape as the hydrostatic shape is increased; the typical shape of the biaxial failure envelope (Fig. 9) and the compression-shear envelope (Fig. 10), etc.

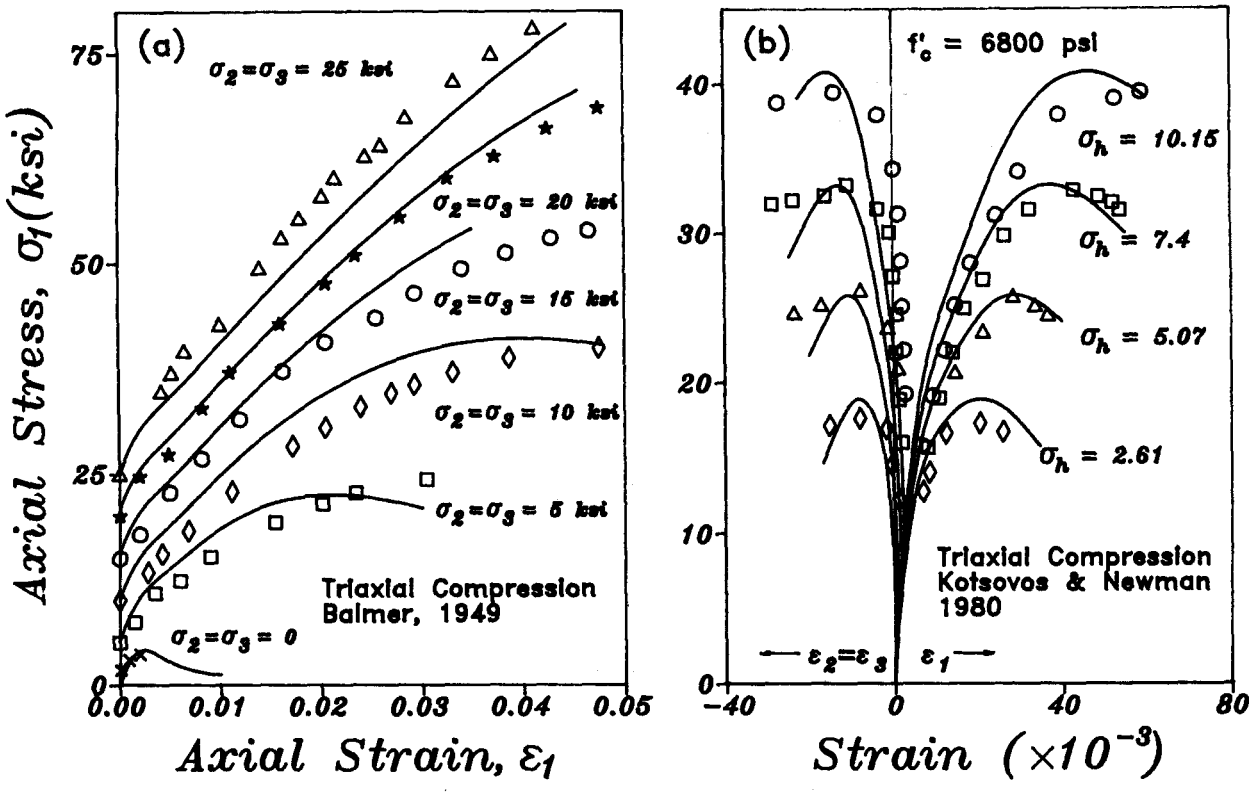

FIG. 5. Comparison with Standard Triaxial Tests, Reported by (*a*) Balmer (1949) (*b*) Kotsovos and Newman (1978)

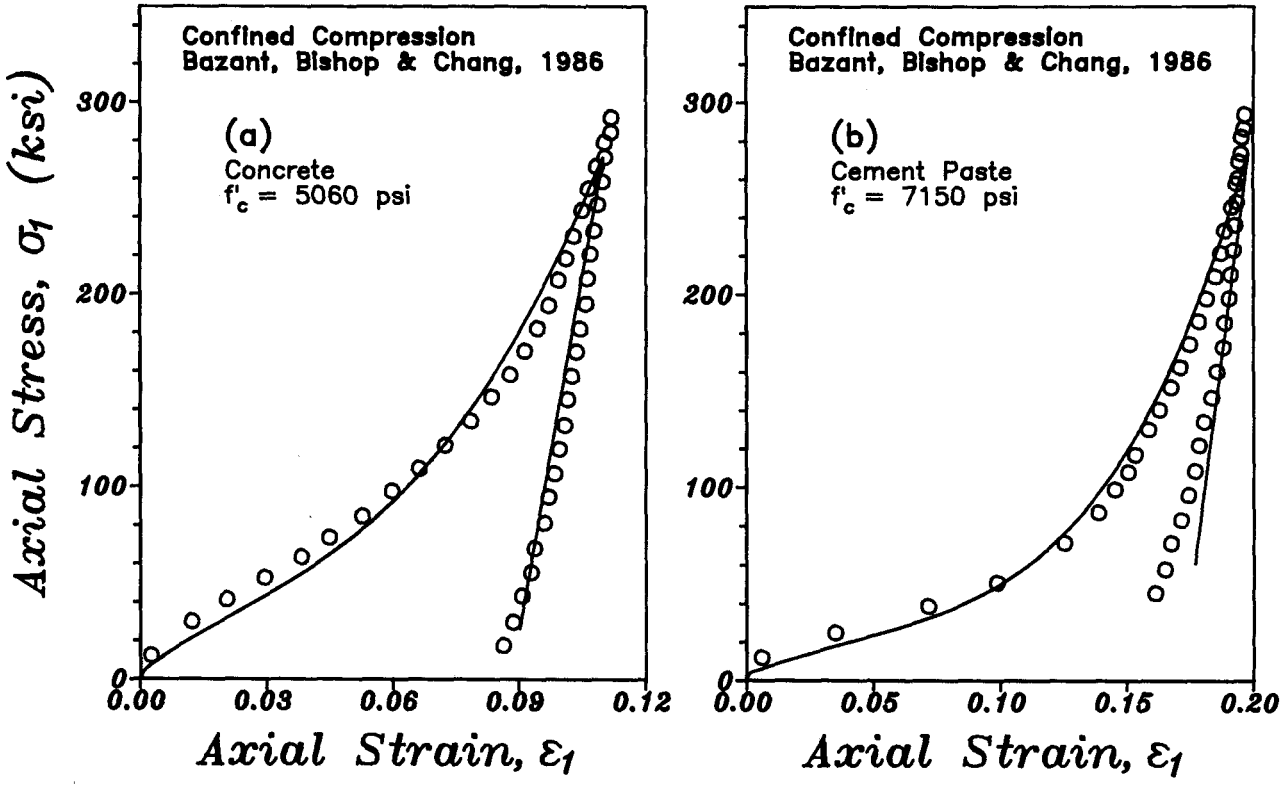

FIG. 6. Comparison with Confined Compression Tests, Reported by Bažant et al.

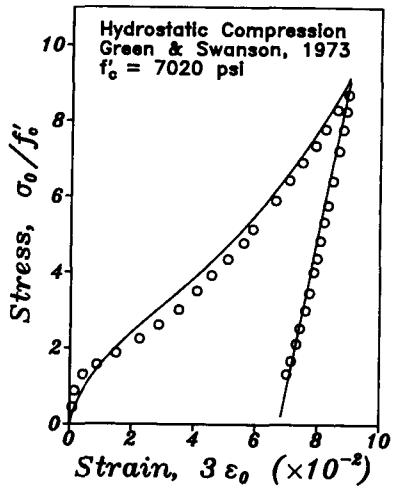

FIG. 7. Comparison with Hydrostatic Compression Tests, Reported by Green and Swanson (1973)

It is interesting to express the initial unloading slope C_u in Fig. 2 as a linear combination of the secant slope C_s and the initial elastic slope C_e [i.e., write $C_u = \xi' C_s + (1 - \xi')C_e$, and calculate $\xi' = (C_u - C_e)/(C_s - C_e)$]. Parameter ξ' is analogous to the material pressure ξ introduced for each microplane (Eq. 5 of Part I). From Fig. 2 we find that $\xi' = 0.57, 0.63, 0.65, 0.66, 0.66$, and 0.67 for the six unloading paths shown (the lowest value of ξ' corresponds to the first unloading). It is surprising that these ξ' values are smaller than the value $\xi = 0.75$ assumed for each microplane (i.e., the macroscopic initial unloading slopes are much closer to the initial elastic slope and much more remote from the secant slope than those for each microplane). The reason is that at the start of unloading only some microplanes start to unload, while some others still continue to load and strain-soften, thus contributing to make the overall macroscopic unloading slope relatively steeper.

Also of interest is to simulate with the present model the responses to various types of loading that are difficult to carry out in the laboratory and on which little or no information is available. Of particular interest is the path dependence of response, especially since assumptions about path independence on the microplane level are central to the present formulation. Fig. 11 (top) shows the responses to the loading paths defined in the figure, in which the final combined state of compressive stress and shear stress is obtained either proportionally or by various nonproportional paths such as uniaxial loading followed by shear. It is seen that the path dependence of the final state reached in these simulations is rather mild.

In the foregoing simulations, the principal stress directions rotate. Fig. 11 (bottom) shows further simulations of responses to loadings in which principal directions do not rotate and are similar to the loading in the cubical true triaxial devices. Shown in these figures are the responses for two principal compressive stresses applied proportionally or in sequence.

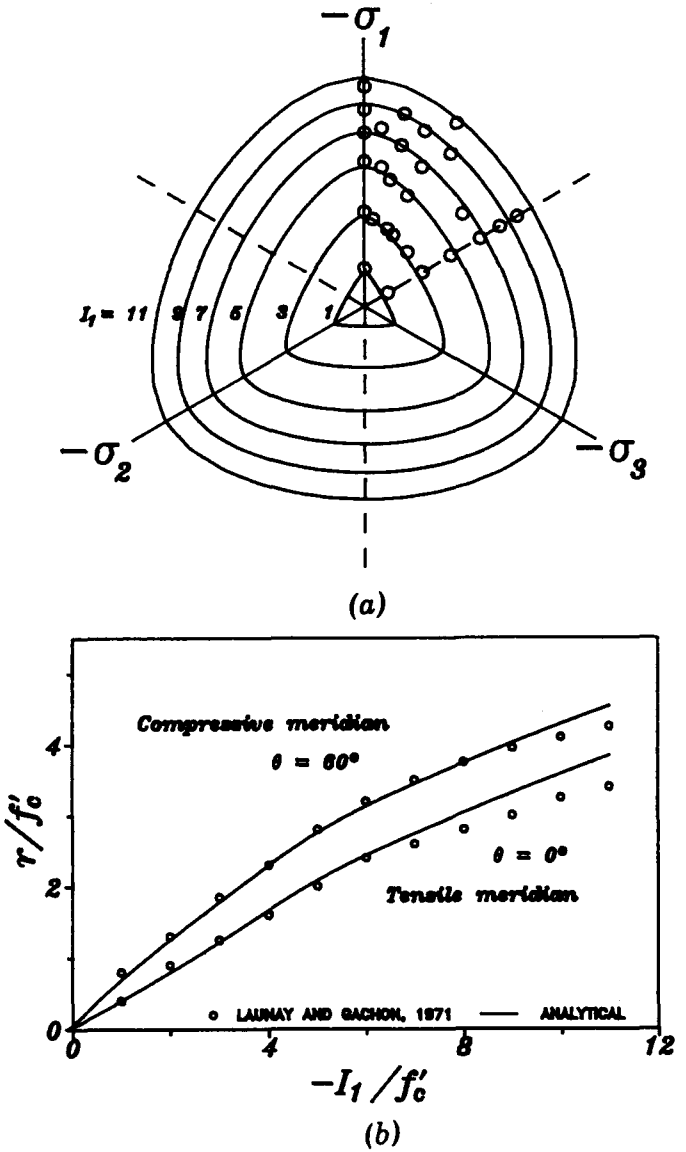

IG. 8. Hydrostatic and Deviatoric Sections of the Failure Surface, Compared to Data Reported by Launay and Gachon (1971)

Interestingly, even though this loading does not reach the softening range, the path dependence appears to be more significant.

One advantage of the present model is its capability to describe compression failure, including the extended strain-softening range, without introducing any maximum stress and strain softening or crushing for

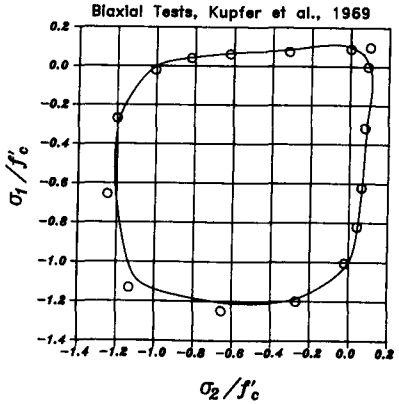

FIG. 9. Biaxial Failure Surface [Data from Kupfer et al. (1969)]

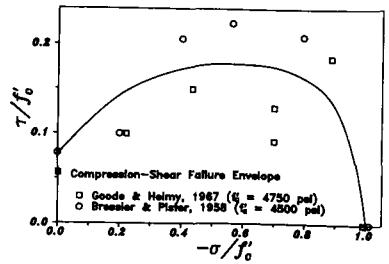

FIG. 10. Compression-Shear Failure Surface [Data from Bressler and Pister (1958) and Goode and Helmy (1967)]

compression on the microplane level. By simulating the uniaxial compression test and recording what happens on various microplanes during the loading process, one finds that the compression failure is obtained as a result of the following sequence: (1) The shear on the inclined planes on a uniaxial test causes slip (inelastic shear strain ε_T) on these planes; (2) the slip on the inclined planes results in a transverse extensional strain, manifested on the microplanes that are parallel to the uniaxial compression axis [Fig. 2(*d*) of Part I]; (3) the transverse extension causes softening in

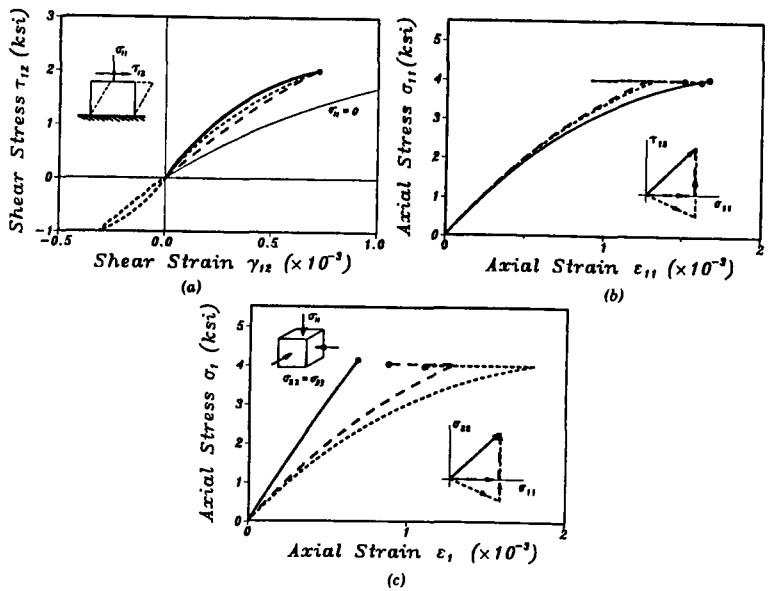

FIG. 11. Top: Path Dependence with Normal and Shear Stresses; Bottom: with only Normal Stresses (True Triaxial Tests)

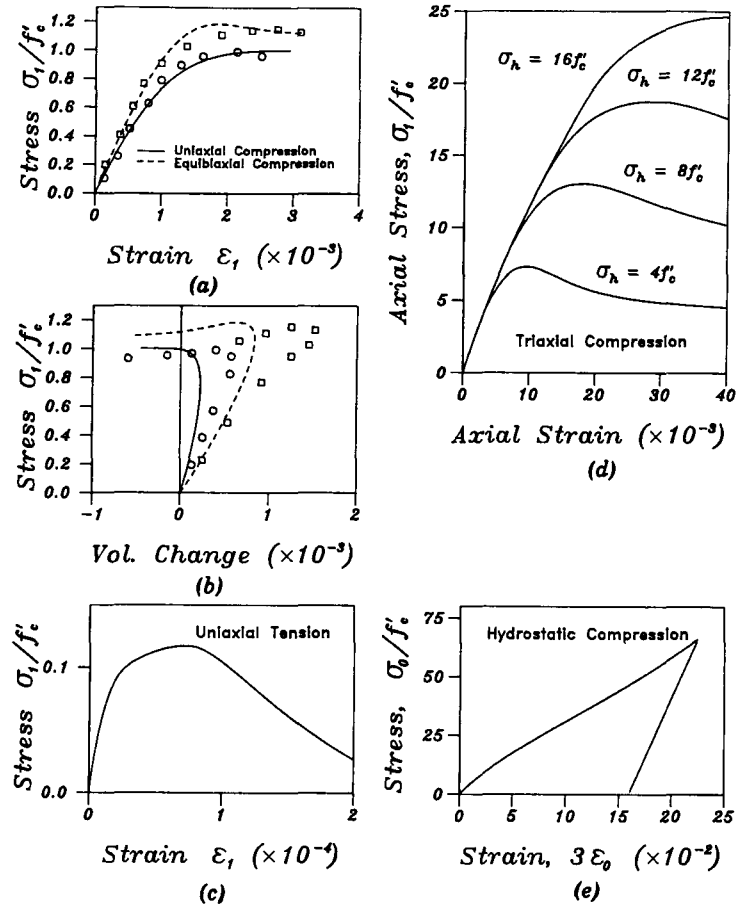

FIG. 12. Prediction of Concrete Response under Different Loading States, using the Parameters Corresponding to the Test Data Reported by Kupfer et al. (1969)

the transverse direction, manifested as splitting microcracks and cracks on planes parallel to the uniaxial compression axis; (4) the loss of resistance in the transverse direction transfers further stress on the inclined microplanes, thus leading to further softening in the transverse direction, etc. Note that if a maximum stress and strain softening were assumed to exist for the compression behavior on the microplane level, it would be impossible to obtain the correct response in the hydrostatic pressure test in which there is no stress peak and no strain softening.

The data sets that exist in the literature (Figs. 1–10) were obtained in different laboratories and therefore somewhat different parameters had to be used to fit each particular data set. Unfortunately, no consensus has been reached on the choice of some standard concrete which would be used in all the laboratories to make the results better comparable. To demonstrate that the response curves are reasonable for all the types of tests considered here (Tables 1 and 2) even if the same material parameters

are used for all the cases, the response curves corresponding to Figs. 1–10 have been run for the parameters of the concrete of Kupfer et al. (1969) (Tables 1 and 2). The curves are shown in Fig. 12.

The test data have been analyzed under the assumption that the deformation in the test specimens during the test was homogeneous. No doubt this was not so in many cases for the strain-softening regime, in which there is always a tendency for localization of strains. In view of this fact, the present formulation is applicable only for describing the behavior of the material elements whose size is roughly equal to the size of the test specimens used. Bodies larger than this have to be subdivided into finite elements of roughly this size in every region where strain softening is expected to occur, and finite elements larger or smaller than this are not allowed in such regions. However, if it is known that the deformation localizes, one can allow for approximate analysis the use of finite elements of a different size (larger or smaller) provided that the strain-softening portion of the stress-strain relation is adjusted so as to maintain the correct value of energy dissipation for the finite elements containing the localized strain-softening zone. This could be formulated in a manner similar to the crack band model for tensile fracture (Bažant and Gambarova 1984).

A general and theoretically sound method for handling strain localization instability due to strain softening is to adopt the recent nonlocal continuum formulation with local strain (Bažant and Pijaudier-Cabot 1987; Bažant et al. 1987; Pijaudier-Cabot and Bažant 1987). The present constitutive model can be implemented in such a nonlocal continuum formulation and this will be one objective of further study.

Conclusion

The conceptual simplicity of the present general microplane model is rewarded by ease of material identification. Several empirical material parameters can be fixed and considered the same for all concretes. Four of the material parameters can be identified independently of the others by simple fitting of a single stress-strain diagram for hydrostatic pressure loading. Finally, there remain only five material parameters that have to be identified by fitting simultaneously the responses measured in various types of triaxial loadings. By contrast, the existing phenomenologic macroscopic models that provide a comprehensive description of the material in many types of tests necessitate over 15 material parameters to be identified by data fitting. Good agreement with the existing basic test data is achieved.

Acknowledgment

The computer implementation and data fitting with the present model has been funded under U.S. National Science Foundation Grant No. MSM-8700830 to Northwestern University.

Appendix. References

Balmer, G. G. (1949). "Shearing strength of concrete under high triaxial stress—computation of Mohr's envelope as a curve." *Struct. Res. Lab. Report No. SP-23*, Denver, Colorado.

Bažant, Z. P. (1987). "Snapback instability at crack ligament tearing and its implication for fracture micromechanics." *Report No. 87-6/498s*, Center for Concrete and Geomaterials, Northwestern Univ., Evanston, Ill.

Bažant, Z. P., and Gambarova, P. G. (1984). "Crack shear in concrete: Crack band microplane model." *J. Struct. Engrg.*, ASCE, 110(9), 2015–2035.

Bažant, Z. P., and Pijaudier-Cabot, G. (1987). "Nonlocal continuum damage, localization instability and convergence." *Report No. 87-2/428n*, Center for Concrete and Geomaterials, Northwestern Univ., Evanston, Ill.

Bažant, Z. P., and Shieh, C.-L. (1978). "Endochronic model for nonlinear triaxial behavior of concrete." *Nucl. Eng. Des.*, 47, 305–325.

Bažant, Z. P., Bishop, F. C., and Chang, T.-P. (1986). "Confined compression tests of cement paste and concrete up to 300 ksi." *J. Am. Concr. Inst.* 33(4), 553–560.

Bažant, Z. P., Lin, F.-B., and Pijaudier-Cabot, G. (1987). "Yield limit degradation: Nonlocal continuum with local strains." *Proc. Int. Conference on Computational Plasticity*, held in Pineridge Press, Swansea, England, 1757–1779.

Bresler, B., and Pister, K. S. (1958). "Strength of concrete under combined stresses." *J. Am. Concr. Inst.*, 551(9), 321–345.

Goode, C. D., and Helmy, M. A. (1967). "The strength of concrete under combined shear and direct stress." *Mag. Concr. Res.* 19(59), 105–112.

Green, S. J., and Swanson, S. R. (1973). "Static constitutive relations for concrete." *Report No. AFWL-TR-72-2*, Air Force Weapons Lab., Kirtland Air Force Base.

Hognestad, E., Hanson, N. W., and McHenry, D. (1955). "Concrete stress distribution in ultimate strength design." *J. Am. Concr. Inst.* 52(4), 455–477.

Kotsovos, M. D., and Newman, J. B. (1978). "Generalized stress-strain relations for concrete." *J. Engrg. Mech.*, ASCE, 104(4), 845–856.

Kupfer, H., Hilsdorf, H. K., and Rüsch, H. (1969). "Behavior of concrete under biaxial stresses." *J. Am. Concr. Inst.* 66, 656–666.

Launay, P., and Gachon, H. (1971). "Strain and ultimate strength of concrete under triaxial stress." *Proc. 1st. Int. Conference on Struct. Mech. in Reactor Technology*, Berlin, West Germany.

Lin, F. B. et al. (1987). "Concrete model with normality and sequential identification." *Comput. Struct.* 26(6), 1011–1026.

Petersson, P. E. (1981). "Crack growth and development of fracture zones in plain concrete and similar materials." *Report No. TVBM 1006*, Lund Inst. of Tech., Sweden.

Pijaudier-Cabot, G., and Bažant, Z. P. (1987). "Nonlocal damage theory." *J. Eng. Mech.* ASCE, 113(10), 1512–1533.

Sinha, B. P., Gerstle, K. H., and Tulin, L. G. (1964). "Stress-strain relations for concrete under cyclic loading." *J. Am. Concr. Inst.* 62(2), 195–210.

van Mier, J. G. M. (1984). "Strain-softening of concrete under multiaxial loading conditions," thesis presented to University Eindhoven, the Netherlands, in partial fulfillment of the requirements for the degree of Doctor of Philosophy.